Lithium-lead corrosion behavior of zirconium oxide coating after heavy-ion irradiation

Lithium-lead corrosion behavior of zirconium oxide coating after heavy-ion irradiation

Sota Miura[1], Kazuki Nakamura[1], Erika Akahoshi[1], Sho Kano[2], Juro Yagi[3], Yoshimitsu Hishinuma[4], Teruya Tanaka[4], Takumi Chikada[1*]

[1]*Shizuoka University, Shizuoka, Japan*
[2]*The University of Tokyo, Tokyo, Japan*
[3]*Kyoto University, Kyoto, Japan*
[4]*National Institute for Fusion Science, Toki, Japan*

For a strict control of tritium migration in fusion reactor fuel systems, tritium permeation barrier coatings have been developed for several decades. In liquid blanket concepts, corrosion of the coatings by liquid tritium breeders is a serious concern in addition to tritium permeation. Furthermore, the coatings are exposed to high-energy neutrons in an actual reactor, which would bring a synergy of irradiation and corrosion. In this study, zirconium oxide (ZrO_2) coatings prepared by metal organic decomposition were exposed to static lithium-lead (Li-Pb) for 500 h at 500−600 ºC after iron-ion irradiation with the damage concentration of up to 16 displacement per atom at room temperature and 500 ºC. Corrosion products formed on all the exposed samples, and their amount and stability depended on the damage density and temperature during irradiation and Li-Pb exposure. Voids were formed by the irradiation and segregated in grain boundaries of the ZrO_2 coating. The thicknesses of irradiated coatings decreased with damage concentration; therefore, Li-Pb corrosion of the coatings would be promoted by microstructure change caused by heavy-ion irradiation. These results suggest that the Li-Pb compatibility of the ZrO_2 coatings would be degraded under irradiation environments.

Keywords: lithium-lead, irradiation, corrosion, coating, zirconium oxide

1. Introduction

In a D-T fusion reactor, tritium must be produced by nuclear reactions between neutron generated from the fusion reaction and lithium installed in a blanket to establish a self-sufficient fuel cycle. However, hydrogen isotopes have high diffusion coefficients in most metals in the operating temperature range, and tritium permeation through blanket materials is a serious issue in terms of the securement of an efficient tritium breeding/recovery system and radiological safety. One of the solutions is to fabricate a functional coating inside the blanket components, and ceramic coatings showed a high reduction performance of hydrogen isotope permeation [1−3]. The functional coating is exposed to neutron and gamma-ray irradiation in the reactor. In particular, neutron irradiation causes defect generation in the coating, leading to a microstructure change and degradation of the permeation reduction performance. The previous studies reported the irradiation effects to ceramic coatings using various heavy ions to simulate the reactor environments [4−7]. In our previous study on iron-ion irradiation to yttrium oxide coatings, the layer formation and an increase in grain size with the damage concentration were confirmed [6].

The functional coating is required especially of liquid blanket concepts which realize a high thermal efficiency with high operating temperatures. Since liquid tritium breeders have high reactivity, the compatibility with blanket materials is also indispensable for the functional coating. The recent studies showed that zirconium oxide (ZrO_2) coatings prepared by a liquid-phase method did not lose their thickness after exposure to liquid lithium-lead (Li-Pb) [8–10]. These results suggest that not only the thermodynamic stability but also the rates of specific reactions between the oxides and Li-Pb affects the Li-Pb compatibility because ZrO_2 has a higher standard free energy of formation than erbium oxide and yttrium oxide. Multiple investigations for the ZrO_2 coating are ongoing for the verification of applicability as a functional coating.

One of the remaining questions to be cleared for the coating is to elucidate a simultaneous effect of irradiation and corrosion which are expected in an actual reactor but cannot be observed in individual studies. In this study, the Li-Pb compatibility of irradiated ZrO_2 coatings was investigated through iron-ion irradiation and static Li-Pb exposure tests.

2. Experimental details

2.1 Sample preparation

Reduced activation ferritic/martensitic (RAFM) steel F82H (Fe-8Cr-2W, F82H-BA07 heat, 25 × 25 × 0.5 mm^3) plates were used as substrates. First, a chromium oxide (Cr_2O_3) layer was formed on the substrate by heat treatment at 710 ºC for 10 min in a quartz tube to prevent peeling of the coating. During the heat treatment, argon and hydrogen mixture gas flowed in the quartz tube with each flow rate of 50 standard cubic centimeters per minute (sccm). ZrO_2 coatings were fabricated by metal organic decomposition (MOD), consisting of dip, dry, pre-heat,

*Corresponding author.
E-mail address: chikada.takumi@shizuoka.ac.jp (T. Chikada)

and heat treatment using a metal-organic liquid precursor (SYM-ZR04, Kojundo Chemical Laboratory Co., Ltd.) [10]. The MOD solution consists of Zr organic salt, 2-ethylhexanoic acid, xylene, and 2-methoxyethanol, and their mass percent are 4−6, 24−29, 65−70, and 0.1−3 %, respectively. The MOD process is described in detail in Ref. [9]. In this study, the dipping, drying, and pre-heat process was repeated 6 times to increase the coating thickness. A series of the MOD process including the heat treatment for crystallization was repeated 2 times. The coating thickness was approximately 700 nm. The coating contained carbon impurity derived from the organic precursor with an atomic concentration of around 15 % [11]. The X-ray diffraction showed that the crystal phase of the coating was the tetragonal or cubic phase, and the estimated grain size was approximately 10 nm. After the coating fabrication, the samples were cut into pieces with a dimension of $4 \times 8 \times 0.5$ mm^3 for the irradiation tests.

2.2 Heavy ion irradiation

The coated samples were irradiated using 2.8 MeV Fe^{2+} by 1.7 MV tandem accelerator at High Fluence Irradiation Facility, The University of Tokyo, HIT. The displacement damages were 0.8, 8, and 16 displacement per atom (dpa), and the irradiation temperatures were room temperature (R.T.) and 500 ºC. Fe-ion beam was focused in the area of 2 mm in diameter. Fe-ion irradiation was simulated using SRIM-2013 codes, with the calculation type of full damage cascades. The threshold displacement energies of Zr, O, and Fe were set at 25, 28, and 25 eV, respectively. Fig. 1 shows a depth profile of the displacement damage of 0.8 dpa to a ZrO_2-coated sample. The damages were fairly uniform in the coating, which was similar to the distribution brought by neutron irradiation. Besides, the depth of the Bragg peak (approximately 1.0 μm) indicated that incident particles did not remain in the coating.

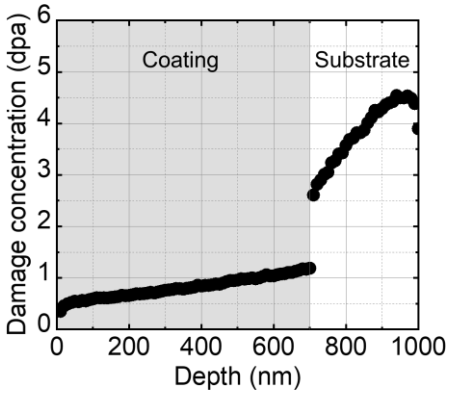

Fig. 1 Depth distribution of damage concentration by irradiation of 2.8 MeV Fe^{2+} in ZrO_2-coated sample with the displacement damage of 0.8 dpa.

2.3 Li-Pb exposure test

Li-Pb with the atomic ratio of Li:Pb = 15.7:84.3 was synthesized from Li (purity: 99.9 %) and Pb (purity: 99.99 %) ingots in the glove box with the argon atmosphere. The irradiated samples were fixed using an iron wire and then sunk into melted Li-Pb in an iron crucible. The crucible was enclosed in a stainless container with a copper gasket. Li-Pb exposure tests were conducted for 500 h at 500 and 600 ºC in an electric furnace. After the exposure tests, the samples were picked up and shook out to remove adhering Li-Pb. No additional cleaning was carried out to avoid damage to the coatings and corrosion products during the cleaning process.

2.3 Li-Pb exposure test

Li-Pb with the atomic ratio of Li:Pb = 15.7:84.3 was synthesized from Li (purity: 99.9 %) and Pb (purity: 99.99 %) ingots in the glove box with the argon atmosphere. The irradiated samples were fixed using an iron wire and then sunk into melted Li-Pb in an iron crucible. The crucible was enclosed in a stainless container with a copper gasket. Li-Pb exposure tests were conducted for 500 h at 500 and 600 ºC in an electric furnace. After the exposure tests, the samples were picked up and shook out to remove adhering Li-Pb. No additional cleaning was carried out to avoid damage to the coatings and corrosion products during the cleaning process.

2.4 Characterization

Surface observations and chemical analyses of the samples were done using a field emission scanning electron microscope (FE-SEM, JSM-7100F, JEOL Ltd.) with energy dispersive X-ray spectroscopy (EDX). Cross-sectional microstructural analyses were performed using a transmission electron microscope (TEM, JEM-2800, JEOL Ltd.) with EDX. The specimens for TEM observations were prepared by a focused ion beam system (FIB, NB5000, Hitachi High-Technologies Co.).

3 Results and discussion

3.1 Surface observation

Fig. 2 shows surface micrographs of the ZrO_2-coated sample before and after Fe-ion irradiation with the displacement damage of 16 dpa. Both surfaces were smooth, and no significant differences were observed; therefore, the surface morphology of the coating did not change by the irradiation damage of up to 16 dpa.

Fig. 3 shows surface micrographs of the samples exposed to Li-Pb for 500 h at 500 ºC before and after irradiation with displacement damages of 0.8, 8, and 16 dpa. The ZrO_2 coatings remained in all the samples, while corrosion product which has a high carbon (C) content

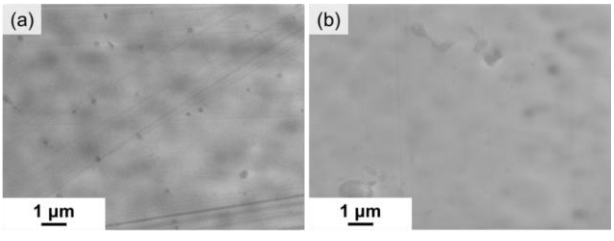

Fig. 2 Surface SEM images of the sample (a) before and (b) after Fe-ion irradiation with a damage concentration of 16 dpa.

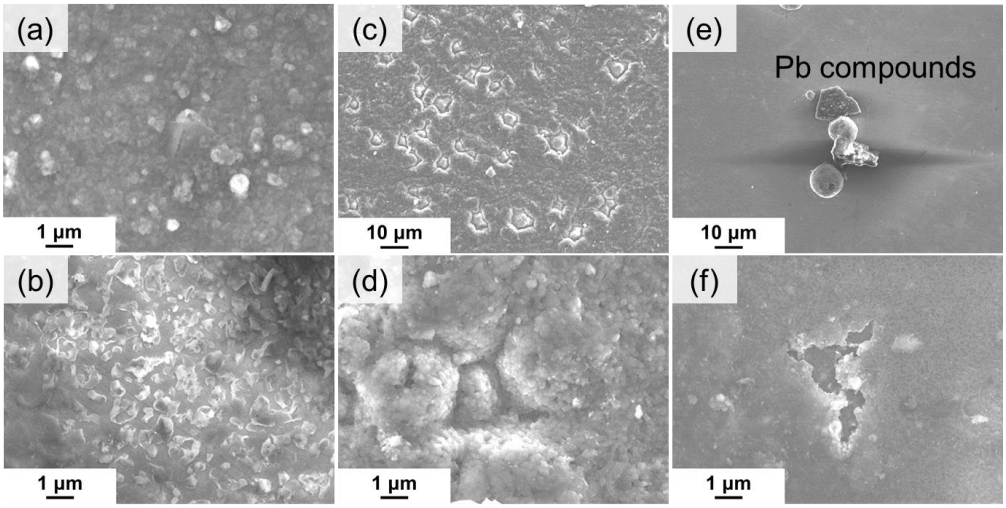

Fig. 3 Surface SEM images of the samples: (a) unirradiated, irradiated with the displacement damage of (b) 0.8 dpa, (c) (d) 8 dpa, and (e) (f) 16 dpa after Li-Pb exposure test for 500 h at 500 ºC.

formed on the ZrO_2 coatings. C was detected on the ZrO_2 coating even before the exposure test; therefore, C in the organic precursor might remain in the coating. Since a lot of C contained in the corrosion product, C might affect the reaction of ZrO_2 and Li. Compared to the unirradiated sample, the grain size of the corrosion product formed on the 0.8-dpa-damaged sample was larger, as shown in Fig. 3(a) and (b). The corrosion product formed more on the 8-dpa-damaged sample, and a thick corrosion product layer with a rough and undulant surface was observed, as shown in Fig. 3(c) and (d). In addition, the corrosion product was collapsed by the electron beam during SEM observation. It is considered that the damage introduction by Fe-ion irradiation promoted the reaction of Li-Pb and the coatings. Although the surface morphology of the coating did not change after irradiation, the amount of defects at the near-surface region increases depending on the displacement damage, leading to the penetration of Li-Pb at the damaged surface. The surface of the 16-dpa-damaged sample was flat in comparison with the 8-dpa-damaged sample as shown in Fig. 3(e) apart from Li compounds at the center of the image. Li compounds were out of consideration in this study because they were observed at all the exposed samples. That discrepancy of the surface structure can be explained that the corrosion product layer was exfoliated in some parts of the 16-dpa-damaged sample as shown in Fig 3(f). The corrosion products formed on the 16-dpa-damaged coating might dissolve and/or delaminate, resulting in a flat surface. This result also indicates that the stability of the corrosion products would depend on the damage concentration.

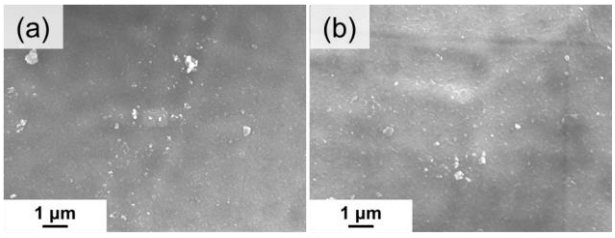

Fig. 4 Surface SEM images of the samples irradiated with the displacement damages of (a) 0.8 and (b) 8 dpa after Li-Pb exposure test for 500 h at 600 ºC.

Fig. 4 shows the surface SEM images of the samples exposed for 500 h at 600 ºC. The samples had a few corrosion products in spite of the damage concentration. In this case, it is assumed that most of the irradiation defects were recovered during the Li-Pb exposure test at 600 ºC due to a higher exposure temperature. No change in surface morphology from the unirradiated sample was also observed.

Fig. 5 shows the surface micrographs of the samples irradiated at 500 ºC and exposed for 500 h at 500 ºC. The surface of the 0.8-dpa-damaged sample had no difference from the unirradiated sample; however, the surface of the 8-dpa-damaged one showed some exfoliations of the corrosion products. This result suggests that the irradiation at a high temperature would make the corrosion products brittle. Irradiation defects were easy to recover at a high temperature. On the other hand, the surface modification of the coating by irradiation at elevated temperature might affect the adhesion of the corrosion product, resulting in the exfoliation of the corrosion product after Li-Pb exposure.

3.2 Cross-sectional observation

Fig. 6 shows the cross-sectional TEM images of the 8- and 16-dpa-damaged samples irradiated at R.T. after Li-Pb exposure for 500 h at 500 ºC. Gaps observed between the coating and the substrate are derived from the Cr_2O_3 layer partly containing a brittle Cr-Fe-O [12]. We consider this formed during fabrication process when the interlayer formation is unavoidable, not during irradiation.

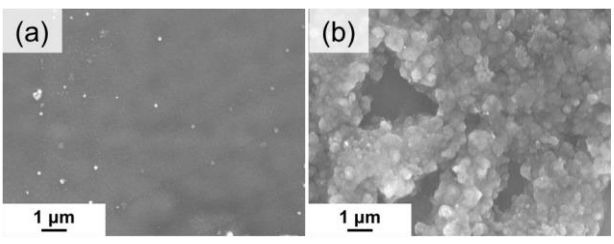

Fig. 5 Surface SEM images of the samples irradiated with the displacement damage of (a) 0.8 and (b) 8 dpa at 500 ºC after Li-Pb exposure test for 500 h at 500 ºC.

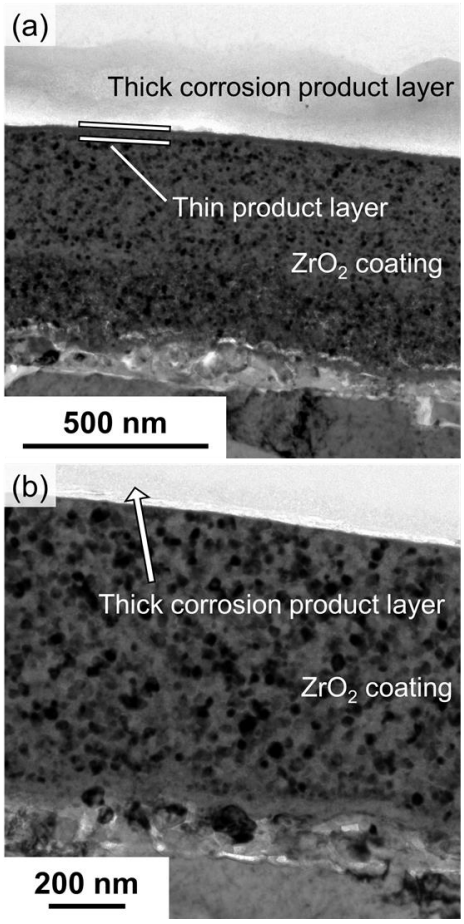

Fig. 6 Cross-sectional TEM images of the samples irradiated with the displacement damage of (a) 8 and (b) 16 dpa at R.T. after Li-Pb exposure test for 500 h at 500 ºC.

These gaps are also observed in our previous study on a pristine yttrium oxide coating deposited by magnetron sputtering [6]. In the 8-dpa-damaged sample, a Cr_2O_3 layer, a ZrO_2 layer, a thin corrosion product layer, and a thick corrosion product layer were observed, and their thicknesses were approximately 70, 540, 10, 230 nm, respectively. An interface in the ZrO_2 layer was observed due to two heat treatments during the coating fabrication. The 16-dpa-damaged coating had a layer structure similar to the 8-dpa-damaged one. The thin corrosion product layer on the 16-dpa-damaged coating was thinner than that on the 8-dpa-damaged coating. The thicknesses of the ZrO_2 layer and the thick corrosion product layer were 450 and 50 nm, respectively. The thickness of the unirradiated ZrO_2 coating did not decrease after Li-Pb exposure in our previous studies [8−10], while those of the damaged coatings after the exposure became thinner than that of the unirradiated one. Therefore, the microstructure change with the Fe-ion irradiation promoted corrosion by Li-Pb.

Fig. 7 shows cross-sectional elemental mappings obtained by EDX for the 8-dpa-damaged sample. The thin corrosion product layer contained Zr, but the thick corrosion product layer did not contain Zr but C and O. Since Li cannot be detected by EDX, the composition of the corrosion products may include Li. The thin corrosion product layer might form by the reaction between ZrO_2 coating and Li. On the other hand, the thick layer might form by the reaction between C including in the coating, Li and O. Fig. 8 shows the thicknesses of the coatings unexposed and exposed to Li-Pb for 500 h at 500 ºC before and after irradiation with the displacement damages of 8 and 16 dpa. The symbol shaped diamond denotes the average value, and the error bar show the range of the minimum and maximum values. In the unirradiated coatings before and after the Li-Pb exposure test, the difference of thickness was within the margin of error. The thicknesses of the 8- and 16-dpa-damaged coatings were smaller than that of the unirradiated one. Moreover, the decrease of the thicknesses depended on the damage density. Fig. 9 shows the enlarged cross-sectional TEM images of the 16-dpa-damaged coating after the Li-Pb exposure test. From the observation of the two images with over focus and under focus, the aligning voids were observed in the coating and also observed in the 8-dpa-damaged coating. These voids distributed around the ZrO_2 grains whose size was approximately 20 nm in diameter, indicating that the irradiation defects segregated in the grain boundaries, indicating that the irradiation defects segregated in the grain boundaries.

From these results, the irradiation defects are considered to promote penetration of Li-Pb into the grain boundaries. The decrease in the coating thickness might be ascribed to the peeling of the coating grain where Li-Pb infiltrated in the grain boundaries. Moreover, the penetration of Li-Pb would progress with the damage density. In the unirradiated coating, the corrosion would

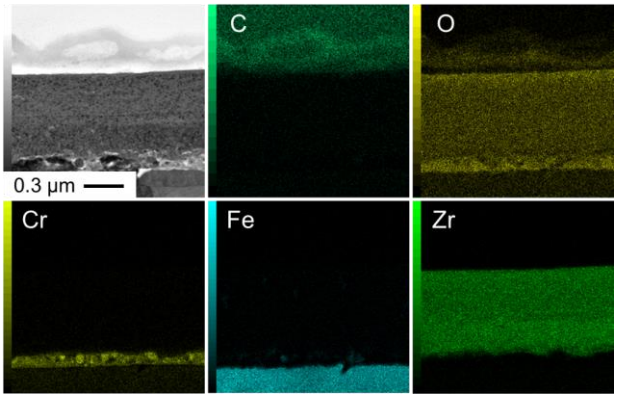

Fig. 7 EDX map of the cross section for the sample irradiated at R.T. with the displacement damage of 8 dpa after Li-Pb exposure test for 500 h at 500 ºC.

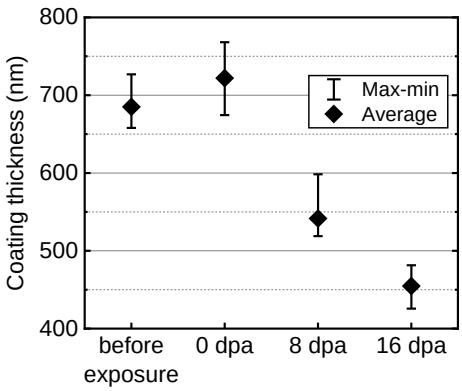

Fig. 8 Coating thicknesses of samples unexposed and exposed to Li-Pb for 500 h at 500 ºC before and after irradiation at R.T.with the displacement damages of 8 and 16 dpa.

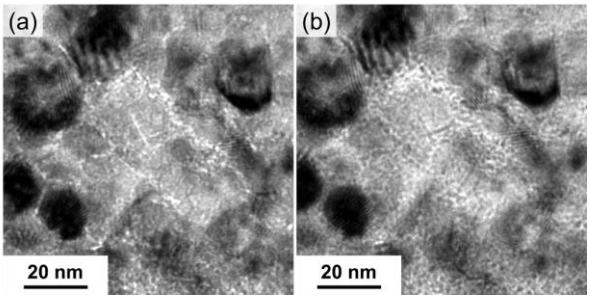

Fig. 9 Enlarged-cross-sectional TEM images of the sample irradiated at R.T. with the displacement damage of 16 dpa after Li-Pb exposure test for 500 h at 500 ºC, at (a) over and (b) under focus.

be proceeded only by the reaction between ZrO_2 and Li. In contrast, the irradiation defects would accelerate the Li-Pb penetration and infiltration, resulting in a decrease in coating thickness. Consequently, the Li-Pb compatibility of the ZrO_2 coatings may deteriorate under irradiation environments.

For a better understanding of the corrosion behavior of the coating, the establishment of how to analyze Li at the interface between Li-Pb and the coating is important. Besides, the parameters of the MOD process such as durations and temperatures of the pre-heating and the heat-treatment should be improved in terms of the removal of carbon impurity in the coating because carbon might affect the reaction of ZrO_2 and Li. As the further experiments, the exposure tests for longer durations are required to obtain more information on the corrosion rate after heavy-ion irradiation. Moreover, deuterium permeation tests under liquid Li-Pb exposure conditions are ongoing to elucidate the effects of irradiation and corrosion on the permeation reduction performance of the functional coating.

4. Conclusion

The Li-Pb exposure tests of the ZrO_2-coated samples after introducing irradiation damage by heavy ions were conducted to elucidate the synergy of irradiation and corrosion. The corrosion products formed in all the samples exposed to Li-Pb, and their amount and stability would depend on the damage concentration. Carbon content in the coating should be strictly controlled to avoid the effect on corrosion. In the Li-Pb exposure tests at 600 ºC, corrosion was mitigated probably by recovery of irradiation defects. The corrosion products were exfoliated in some parts at the sample irradiated at 500 ºC and exposed at 500 ºC. Not only irradiation defects but also thermal stress would vary the corrosion behavior. Voids formed by the iron ion irradiation segregated in grain boundaries of ZrO_2 coatings and would promote penetration of Li-Pb along the grain boundaries. The thicknesses of irradiated coatings decreased in comparison with that of the unirradiated one, which indicates that microstructure changes brought by heavy-ion irradiation promotes Li-Pb corrosion. The synergy of irradiation and corrosion should be taken into consideration for the application of the ZrO_2 coating as a functional coating in the Li-Pb blanket system.

Acknowledgments

This work was supported by JSPS KAKENHI Grant Number 19H01873, the general collaboration research with National Institute for Fusion Science (NIFS18KEMF119) and a collaborative research project at Nuclear Professional School, School of Engineering, The University of Tokyo.

References

[1] G.W. Hollenberg et al., Tritium/hydrogen barrier development, Fusion Eng. Des. 28 (1995) 190–208.

[2] J. Konys et al., Status of tritium permeation barrier development in the EU, Fusion Sci. Technol. 47 (2005) 844–850.

[3] T. Chikada, Ceramic Coatings for Fusion Reactors, In: R. Konings and R. Stoller (eds.), Comprehensive Nuclear Materials 2nd edition 6 (2020) 274–283, Oxford: Elsevier.

[4] Y. Hishinuma et al., Microstructure and peeling behavior of MOCVD processed oxide insulator coating before and after ion beam irradiation, Nucl. Mater. Energy 16 (2018) 123–127.

[5] F. García Ferré et al., Extreme ion irradiation of oxide nanoceramics: Influence of the irradiation spectrum, Acta Mater. 143 (2018) 156–165.

[6] K. Nakamura et al., Iron-ion irradiation effects on microstructure of yttrium oxide coating fabricated by magnetron sputtering, Fusion Eng. Des. 146 (2019) 2031–2035.

[7] K. Nakamura et al., Effects of helium implantation with heavy ion irradiation on deuterium permeation in yttrium oxide coating, J. Nucl. Mater. 537 (2020) 152244.

[8] M. Matsunaga et al., Lithium-lead corrosion behavior of erbium oxide, yttrium oxide and zirconium oxide coatings fabricated by metal organic decomposition, J. Nucl. Mater. 511 (2018) 537–543.

[9] E. Akahoshi et al., Corrosion tests of multi-layer ceramic coatings in liquid lithium-lead, Fusion Eng. Des. 160 (2020) 111974 (6pp).

[10] J. Mochizuki et al., Preparation and characterization of Er_2O_3-ZrO_2 multi-layer coating for tritium permeation barrier by metal organic decomposition, Fusion Eng. Des. 136 (2018) 219–222.

[11] S. Nakazawa et al., Gamma-ray irradiation effect on deuterium retention in reduced activation ferritic/martensitic steel and ceramic coatings, J. Nucl. Mater. 539 (2020) 152321.

[12] T. Chikada et al., Compatibility of tritium permeation barrier coatings with ceramic breeder pebbles, Corros. Sci. 182 (2021) 109288.